Constrained evolution of a core winter proteome across independently cold-adapted PACMAD grasses

Authors

Elad Oren[1*], Jingjing Zhai[1], Travis E Rooney[2], Ruthie Angelovici[3], Charles O. Hale[4], Lara J. Brindisi[1,6], Sheng-Kai Hsu[1], Christine M. Gault[1], Jian Hua[5], Thuy La[1], Nicholas Lepak[6], Qin Fu[7], Edward S. Buckler[1,6], M. Cinta Romay[1*]

Affiliations

1. Institute for Genomic Diversity, Cornell University, Ithaca, NY 14853, USA
2. Sesaco Corporation, Austin, TX 78701, USA
3. Division of Biological Sciences and Interdisciplinary Plant Group, University of Missouri, Columbia, Missouri, 65211, USA
4. School of Integrative Plant Sciences, Plant Breeding and Genetics Section, Cornell University, Ithaca, New York, 14853, USA
5. School of Integrative Plant Science, Plant Biology Section, Cornell University, Ithaca, New York, 14853, USA
6. USDA-ARS, Ithaca, NY, USA 14853
7. Proteomics and Metabolomics Facility, Cornell University, Ithaca, New York, 14850, USA

***Corresponding authors:**

Elad Oren

Tel: +972 49539517

Email: eladoren@volcani.agri.gov.il

M. Cinta Romay

Tel: +1 607-255-1809

Email: mcr72@cornell.edu

The author responsible for distribution of materials integral to the findings presented in this article is Elad Oren.

Total word count (excluding summary, references and legends):	6,351	No. of figures:	5 (Figs 1–5)
Summary:	200	No. of Tables:	1 (Table 1)
Introduction:	705	No. of Supporting Information files:	4 (Figs S1–S10; Tables S1–S13; Methods S1; Code S1–S3)
Materials and Methods:	2,465		
Results:	1,466		
Discussion:	1,263		
Acknowledgements:	252		

Summary

- Grasses in the PACMAD clade independently colonized cold environments from warm-climate ancestors, but whether their molecular responses to freezing reflect shared evolutionary solutions or lineage-specific innovations remains unknown. We used comparative proteomics to test whether protein-level cold responses show stronger cross-species conservation than previously observed at the transcript level.

- We quantified seasonal rhizome proteomes (winter vs summer) from five PACMAD species grown in a common garden exposed to sustained sub-zero temperatures, identified differentially abundant proteins, and compared fold-change magnitudes across species using orthogroup-based correlation analyses. We further examined LEA3 protein structure through hydropathy profiling and motif analysis.
- Shared cold-responsive proteins showed higher cross-species fold-change correlation (ρ = 0.80) than background proteins (ρ = 0.45), despite greater divergence in baseline abundance. LEA3 was the only ortholog elevated across all five species. Cold-tolerant species contained more tandem 11-mer repeats than the cold-sensitive maize, and two species accumulated multiple LEA3 paralogs, increasing total LEA3 abundance.
- Independent evolution of freezing tolerance in PACMAD grasses is governed by evolutionary constraints on protein-level response magnitude, reflecting the retention of an ancestral protective capacity. Structural divergence of LEA3 in maize suggests that transcriptional induction alone does not ensure freezing tolerance; functional protection likely requires intact motif architecture.

Keywords: Cold acclimation, Constrained evolution, Freezing tolerance, LEA proteins, PACMAD grasses, Proteomics, Rhizome, Tripsacum.

Introduction

Maize (*Zea mays* ssp. mays), a vital crop for global food security, is susceptible to cold stress due to its tropical origins, limiting its yield in temperate regions. Early planting of maize can improve nitrogen capture, net primary productivity, and yield (Ojeda-Rivera et al., 2025). However, this strategy requires cold tolerance, which is lacking in current elite maize varieties (Lyons, 1973; Aroca et al., 2012). Cold and freezing tolerance has arisen independently multiple times within the Panicoideae, Aristidoideae, Chloridoideae, Micrairoideae,

59 Aristavideae, and Danthonioideae (PACMAD) clade, a major lineage of predominantly C4
60 grasses (*Poaceae*) that diverged ~64 Mya, with ancestral roots in the Afrotropics (Sage et al.,
61 2011; Gallaher et al., 2022). These parallel origins of freezing tolerance provide a natural
62 comparative framework. Among these, *Tripsacum*, the closest perennial and cold-tolerant
63 relative of maize, having diverged about 650 Kya (Chen et al., 2022), is valuable for enhancing
64 maize cold tolerance.

65 PACMAD grasses originated in warm-season climates unlike temperate diversified Pooideae
66 and Danthonioideae (Kellogg, 2015). However, most transitions of PACMAD grasses to colder
67 climates occurred in tropical mountains, where cold-adapted lineages converged with
68 temperate migrants (Schubert et al., 2020). Each PACMAD genus exhibits distinct
69 evolutionary trajectories, polyploid histories, and biogeographic origins, having independently
70 evolved robust cold and freezing tolerance over the past 20-30 million years (Fig. 1e; Gallaher
71 et al., 2022; Stitzer et al., 2025).

72 Plant exposure to cold stress, including chilling (>0°C) and freezing (<0°C) temperatures,
73 triggers physiological and molecular responses. Chilling stress disrupts membrane fluidity,
74 impairs enzyme activity, and inhibits photosynthesis (Aroca et al., 2012), whereas freezing
75 stress induces ice crystal formation in extracellular spaces, leading to cellular dehydration,
76 membrane damage, and ultimately, cell death (Pearce, 2001). Many temperate plants undergo
77 cold acclimation, resulting in adaptations such as membrane lipid modifications (Degenkolbe
78 et al., 2012; Barnes et al., 2016), accumulation of compatible solutes (Koster & Lynch, 1992),
79 enhanced antioxidant enzyme activity (Suzuki & Mittler, 2006) and protective protein
80 accumulation (Puhakainen et al., 2004; Xu et al., 2022). Plant cold perception involves plasma
81 membrane modifications, including fluidity changes, Ca^{2+} channel activation, and cytosolic
82 acidification, driving lipid and transcriptomic responses (Mori et al., 2018; Barnes et al., 2023).

83 A widely conserved mechanism underpinning freezing tolerance is the activation of the C-
84 repeat binding factor/dehydration-responsive element-binding (CBF/DREB) signaling
85 pathway, which induces expression of cold-responsive (COR) genes (Thomashow, 1999;
86 Nakashima & Yamaguchi-Shinozaki, 2006).

87 Studies in PACMAD grasses reveal both broadly conserved and species-specific molecular
88 adaptations associated with this pathway. *Panicum virgatum* utilizes a zinc finger transcription
89 factor, PvC3H72, to enhance ICE1-CBF-COR signaling, significantly increasing cold
90 resilience (Xie et al., 2019). Additionally, calcium signaling pathways involving calmodulin
91 and MEKK1 provide early response to cold stress (Ranaweera et al., 2022; Wu et al., 2024).
92 *Pennisetum giganteum* maintains membrane fluidity at low temperature through the
93 accumulation of unsaturated fatty acids, such as linoleic and α-linolenic acids (Zhang et al.,
94 2017; Li et al., 2020). Protective proteins, such as late embryogenesis abundant (LEA) proteins,
95 dehydrins, and antioxidant enzymes, are accumulated in response to freezing conditions,
96 reducing oxidative injury and cellular dehydration (Liu et al., 2016; Xie et al., 2019). Species-
97 specific adaptations include enhanced proline biosynthesis via the ornithine pathway in
98 *Sorghum bicolor* (Vera-Hernández et al., 2018) and elevated activity of phenylpropanoid
99 pathway enzymes (PAL and CAD) in *Miscanthus* to protect cells during freezing stress
100 (Domon et al., 2013).

101 Previous studies in PACMAD grasses have focused mainly on transcriptomic and metabolomic
102 adaptations. However, proteomic responses remain largely unexplored. As the functional
103 products of genes, proteins integrate transcriptional, translational, and post-translational
104 regulation. Given the persistent nature of cold stress, proteomic analysis uniquely captures the
105 accumulation of proteins reflecting acclimation and sustained adaptive responses. Furthermore,
106 Cope et al. (2025) demonstrated that proteins face stronger evolutionary constraints than

107 transcripts, with protein abundances being highly conserved across species while mRNA levels
108 can vary without substantially affecting protein output. This suggests that shared cold adaptive
109 responses may be more readily detected at the protein level than at the transcript level, making
110 proteomics essential for understanding adaptive processes such as those underlying cold or
111 freezing tolerance. Our multi-species study examines rhizome protein accumulation across
112 seasonal variation to identify conserved freezing-tolerance mechanisms in PACMAD grasses,
113 testing whether freezing tolerance across these lineages reflects retention of shared ancestral
114 molecular responses or lineage-specific innovations.

115 **Materials and Methods**

116 To investigate proteomic responses to seasonal changes across PACMAD grasses, we
117 conducted a comparative analysis of rhizomes from five species under winter (January, with
118 lows reaching –29°C) and summer (August, with highs of 26°C) conditions. The species
119 analyzed (Fig. 1a) were interspecific and intraspecific hybrids of *Tripsacum dactyloides* (L.)
120 L. and *Tripsacum floridanum* Porter ex Vasey, *Andropogon gerardi* Vitman (cv. 'Sentinel'),
121 *Miscanthus* × *giganteus* J.M.Greef & Deuter ex Hodk. & Renvoize, *Panicum virgatum* L. (cv.
122 'Dust Devil'), and *Sorghastrum nutans* (L.) Nash (cv. 'Golden Sunset').

123 *Phylogenetic context of freezing tolerance*

124 To illustrate independent origins of freezing tolerance in each of the five study species rather
125 than from a single common ancestor, we constructed phylogenetic context by pruning the
126 1,153-tip ASTRAL-Pro nuclear species tree (Arthan et al., 2024) to 14 representative species
127 (Fig. 1e): Paniceae (2 species) and Andropogoneae (11 species from 7 subtribes) and
128 *Eragrostis tef* (Chloridoideae) as outgroup. Of these 14, only five temperate species were
129 sampled for proteomics analysis (*P. virgatum*, *T. dactyloides*, *S. nutans*, *A. gerardi*, and *M.*
130 *giganteus*); the remaining nine tropical relatives (*Megathyrsus maximus*, *Zea mays*, *Coix*

lacryma-jobi, *Themeda triandra*, *Cymbopogon citratus*, *Hyparrhenia hirta*, *Sorghum bicolor*, *Saccharum officinarum*) were included to demonstrate that each study species sits on a separate branch from its nearest warm-climate relative, confirming five independent transitions to freezing tolerance. *Sorghastrum fuscescens* served as a positional proxy for *S. nutans*, which was absent from the tree, and *M. giganteus's* position was determined by its maternal progenitor, *Miscanthus sinensis*. Thermal ecology was classified as tropical or temperate based on native range descriptions in Kellogg (2015).

Plant material and environmental conditions

Plants were grown outdoors at two field sites in Ithaca, New York (USDA Hardiness Zone 6a), where they experienced natural seasonal fluctuations, with an average winter temperature of –5°C (lows reaching –29°C) and summer temperatures averaging 20°C (highs of 26°C) over the five years preceding sampling (Northeast Regional Climate Center, 2025). *Tripsacum* hybrids were cultivated at Cornell University Caldwell Field, while *A. gerardi, M. giganteus, P. virgatum*, and *S. nutan*s were grown at the Cornell Botanic Gardens. Environmental data were obtained from the Northeast Regional Climate Center (Station USC00304174) and the New York State Mesonet (Station GROT; Brotzge et al., 2020).

Sampling and experimental design

Rhizome tissue was collected during two sampling campaigns in 2019-2020 and 2022, timed to capture distinct physiological states: winter dormancy and summer active growth. Summer samples were collected in August 2019 and August 2022 during active growth; winter samples in January 2020 and December 2022 during dormancy. Soil temperatures and precipitation data for each sampling date are reported in Supporting Information Methods S1.

153 At summer sampling, plants displayed active vegetative rhizome growth with no visible
154 drought stress; winter samples were dormant with hardened exteriors (Fig. S1). Our study was
155 conducted in two phases. Initial sampling of *Tripsacum* hybrids in 2019 provided evidence of
156 conserved winter protein accumulation, prompting expansion in 2022 to both replicated
157 *Tripsacum* sampling and four additional PACMAD species with independent evolutionary
158 histories of cold adaptation.

159 Rhizome tissue (minimum 5 g fresh weight) was collected from the internal mid-sections of
160 rhizomes using sterile pruning scissors. Sampling was standardized to exclude apical tips, fine
161 roots, and necrotic zones to ensure reproducibility and tissue comparability across species (Fig.
162 1c and Fig. S1). Samples were immediately placed in pre-labeled 15 ml tubes, transported on
163 dry ice, and stored at −80°C within 4 hours of collection. Biological replicates were defined as
164 tissue collected from independent clonal plants. Sample sizes and genotypes are detailed in
165 Table 1. For *A. gerardi* ('Sentinel'), *M. giganteus*, and *P. virgatum* ('Dust Devil'), three
166 biological replicates were sampled per season from established accessions at Cornell Botanic
167 Gardens. *S. nutans* ('Golden Sunset') was represented by two biological replicates per season
168 due to winter mortality of one clonal plant.

169 *Tripsacum hybrid population*

170 *Tripsacum* rhizomes were sampled from seven-year-old F_1 hybrid progenies that had survived
171 multiple freezing winters at Cornell University's Caldwell Field. The hybrids were derived
172 from controlled crosses between northern founders collected from Iowa, Kansas, Illinois, and
173 Missouri, where winters experience heavy frost, and southern founders collected from Florida
174 and Texas, with subtropical climates. Most crosses were interspecific, between *T. dactyloides*
175 subsp. *dactyloides* (northern) and *T. floridanum* (southern); additional crosses were
176 intraspecific, between northern and southern populations of *T. dactyloides* (Table 1). In 2019,

177 we sampled eight individuals per season representing six distinct hybrid genotypes from five
178 cross combinations, prioritizing coverage of genetic diversity across the hybrid population. In
179 2022, we sampled 24 individuals per season comprising eight hybrid genotypes with three
180 clonal replicates each, balancing genetic diversity with robust statistical replication.

181 *F_2 Seedlings for RNA sequencing*

182 F_2 seeds used for seedling freezing tolerance screening and RNA sequencing were generated
183 from the same *Tripsacum* hybrids described above. Due to the limited seed set achieved
184 through self-pollination (~500 seeds over the entire season), F_1 plants were allowed to open-
185 pollinate. Seeds were harvested from individual maternal plants, germinated in trays, and
186 grouped into F_2 families based on maternal lineage. Six-week-old F_2 seedlings sharing the same
187 maternal F_1 parent were selected as experimental material for freezing assays and RNA
188 extraction.

189 *Proteomics data*

190 Proteomic profiling was conducted using tandem mass tag (TMTpro) labeling and Orbitrap
191 Eclipse Real Time Search (RTS)-SPS-MS^3 technology. The experimental design included
192 samples collected in both winter (January) and summer (August), with each species represented
193 by at least three biological replicates with a larger number of genotypes analyzed for *Tripsacum*
194 across two years (see Table 1 and Fig. 1d).

195 *Protein Extraction and Digestion*

196 Fresh rhizome tissue was ground in liquid nitrogen and subjected to phenol-based protein
197 extraction with protease and phosphatase inhibitors, followed by ammonium acetate/methanol
198 precipitation. Protein pellets were dissolved in 8 M urea, quantified by BCA assay, and digested
199 using the S-Trap protocol with trypsin. Digested peptide mixtures were labeled using TMTpro

200 reagents: TMTpro 16-plex for 2019 Tripsacum samples and TMTpro 18-plex for 2022 samples.
201 The 2022 samples were processed across seven separate TMTpro 18-plex batches: four batches
202 for Tripsacum and three batches for the remaining four species, with winter and summer
203 samples from each species always included within the same batch. Detailed buffer
204 compositions, wash steps, digestion parameters, and labeling procedures are provided in
205 Supporting Information Methods S1.

206 *LC-MS/MS analysis and database searching*

207 Labeled peptides were fractionated by high-pH reversed-phase chromatography (48 fractions
208 concatenated into 10 pools) and analyzed by nanoLC coupled to an Orbitrap Eclipse mass
209 spectrometer using the RTS-SPS-MS^3 method (Fu et al., 2021). Raw data were processed in
210 Proteome Discoverer 2.5 using the Sequest HT search engine against species-specific reference
211 proteomes (see Peptide Mapping and Reference Proteome Assignment). Peptide spectral
212 matches were filtered at 1% FDR (Percolator), and protein identifications required a minimum
213 of two distinct peptides. Protein quantification was based on summed reporter ion intensities
214 of unique and razor peptides. Full search parameters, modification lists, mass tolerances, and
215 reporter ion filtering criteria are detailed in Methods S1.

216 Given the inherent biological variability of a multi-species field study, we applied a stringent
217 threshold for differential abundance. Differentially abundant proteins (DAPs) were determined
218 based on $|\log_2 \text{fold change}| \geq 1$ and adjusted P-value < 0.05, to prioritize high-confidence
219 candidates with robust seasonal responses over minor fluctuations that may reflect transient
220 environmental noise rather than conserved adaptive strategies. This approach helps address the
221 statistical power imbalance between the deeply sampled Tripsacum dataset ($n \approx 32$) and the
222 other grass lineages ($n=3$). While the higher power in Tripsacum inherently yields a larger list
223 of statistically significant changes, our comparative analysis defines conservation based on the

224 intersection of species. Consequently, the identification of conserved proteins is constrained
225 by the more limited statistical power of the smaller datasets, suggesting that the core response
226 network we report represents a high-confidence set of shared adaptations rather than an
227 exhaustive catalog.

228 *Peptide Mapping and Reference Proteome Assignment*

229 Initial Sequest HT searches were performed against species-specific reference proteomes (see
230 above). For species pooled within the same TMT batch due to <15% predicted proteome
231 divergence, such as *A. gerardi* and *M. giganteus*, spectra were searched against the *A. gerardi*
232 proteome. To improve protein recovery for *M. giganteus*, peptides were re-mapped to the *M.*
233 *sinensis* proteome using DIAMOND BLASTp in "ultrasensitive" mode. Proteins were
234 reassigned to their best-matching *M. sinensis* counterparts based on aggregated peptide
235 evidence (see Supporting Information Code S1–S3; GitHub repository).
236 All final analyses were conducted using species-specific reference proteomes: *Andropogon*
237 *gerardi* (Ag-CAM1351-DRAFT-PanAnd-1.0), *Miscanthus* × *giganteus*
238 (Msinensis_497_v7.0), *Panicum virgatum* (Pvirgatumvar_WBCHAP1_778_v1.0),
239 *Sorghastrum nutans* (Sn-CAM1369-DRAFT-PanAnd-1.0), and *Tripsacum dactyloides* (Td-
240 FL_9056069_6-DRAFT-PanAnd-1.0); genome assemblies and annotations are listed in the
241 Data Availability section.

242 *Protein abundance normalization and statistical analysis*

243 Protein intensities were normalized using the "total peptide amount" method in Proteome
244 Discoverer 2.5. Differential abundance between winter and summer was assessed using one-
245 way ANOVA followed by Tukey's HSD post hoc test, with multiple testing correction by the
246 Benjamini-Hochberg procedure. For the multi-batch *Tripsacum* 2022 dataset, statistical testing
247 was performed within each batch and P-values were combined using Fisher's method; only

248 proteins quantified in at least 3 of 4 batches were retained. Proteins quantified in both seasons
249 within each species were considered differentially abundant at $|\log_2 FC| \geq 1$ and adjusted $P <$
250 0.05.

251 PCA was performed on $\log_2$-transformed protein abundances (Table S1) and on orthogroup-
252 level data detected in >50% of samples per species (Fig. S2). For Tripsacum, batch effects were
253 removed via residuals from a linear model prior to PCA; because season was the dominant
254 factor (Fig. S2b), all Tripsacum samples were pooled across years. For cross-species
255 comparison, orthogroups were assigned using OrthoFinder (Emms & Kelly, 2019), with fold-
256 change values averaged when multiple proteins mapped to the same orthogroup. All analyses
257 were performed in R v4.4.3.

258 *Cross-species correlation analysis*

259 To assess evolutionary constraint on cold-responsive proteins, we compared cross-species
260 conservation of seasonal response magnitude between shared cold-responsive orthogroups and
261 background proteins, following the framework of Cope et al. (2025).

262 For each orthogroup quantified in at least four of five species, we calculated pairwise Spearman
263 correlations of $\log_2$ fold-change (winter/summer) across all species pairs. Orthogroups were
264 classified as "shared DAPs" if differentially abundant ($|\log_2 FC| \geq 1$, adjusted $P < 0.05$) in two
265 or more species, or as "background" if differentially abundant in at most one species.
266 Distributions of pairwise correlations were compared between shared DAPs and background
267 using the Wilcoxon rank-sum test. The same approach was applied to basal protein abundance
268 (summer and winter separately) to distinguish constraint on response dynamics from constraint
269 on absolute abundance levels.

Functional annotation and GO enrichment

Orthogroups were assigned using OrthoFinder (v2.5.5; Emms & Kelly, 2019), with DIAMOND (v2.1.9; Buchfink et al., 2021) for all-vs-all sequence comparisons across all five species. Orthogroups served as the basis for cross-species comparisons and functional propagation of annotations. DAP sequences were annotated using DIAMOND BLASTp against the SwissProt with gene ontology (GO) terms extracted from UniProt. For DAPs lacking SwissProt hits, functional predictions were generated using PANNZER2 (Törönen & Holm, 2022), run independently for each species. Annotation of non-significant proteins is detailed in Methods S1.

GO term enrichment analysis was performed using the topGO R package (v2.50.0; Alexa & Rahnenfuhrer, 2017), with the "elim" algorithm with Fisher's exact test, separately for winter-elevated and winter-reduced proteins against all quantified proteins. Terms with a minimum node size of 10 and a P-value < 0.01 were considered significant. Due to the hierarchical nature of topGO's algorithm, multiple test correction was not necessary (Alexa & Rahnenfuhrer, 2017).

Candidate protein exploration methods

Barnes et al. (2023) showed that cold-responsive transcriptional and proteomic changes often overlap with broader stress mechanisms involving damage, osmotic imbalance, and acidification. To improve biological resolution, we curated DAPs into nine functional categories based on known roles in freezing tolerance (Orvar et al., 2000; Iwaya-Inoue et al., 2018; Schubert et al., 2020): (1) protein aggregation and membrane stability, (2) protein folding and chaperone activity, (3) metabolism and osmoregulation, (4) detoxification and ROS scavenging, (5) lipid metabolism, (6) antifreeze and cell wall modification, (7) cold signal transduction, (8) cytoskeletal organization, and (9) other/uncategorized. Assignments were

294 informed by protein descriptions, GO terms, PANNZER2 predictions, and domain feature
295 review (Fig. S3).

296 *Selecting proteins for traits on trees*

297 Proteins for phylogenetic trait mapping were identified by text-mining PANNZER2
298 annotations for GO terms associated with LEA proteins, HSPs, and EF1. Full-length sequences
299 were extracted from reference proteomes using seqkit grep (v2.0), aligned with MAFFT
300 (v7.475), and used to infer maximum-likelihood trees with raxmlHPC (RAxML-8.2.13,
301 `PROTGAMMAJTT`, 100 bootstraps). Trees were rooted on appropriate outgroups and visualized
302 with ggtree, mapping $\log_2$FC values as tip-point colors. Alignment and tree-building
303 parameters are detailed in Methods S1.

304 *RNA-seq processing and differential expression analysis*

305 Transcriptome data for maize chilling responses across tissues (leaf, root, top-crown, and
306 bottom-crown) were derived from Xue et al. (2021) using 3′ RNA-seq (5C vs. 22C). For
307 *Tripsacum*, we analyzed leaf transcriptome data from a segregating freezing-tolerant bulk of
308 F_2 seedlings derived from the same *Tripsacum* hybrids used in our rhizome analysis. Plants
309 from seven F_2 families were bulked as freezing-tolerant or intolerant based on survival after
310 exposure to -8°C for three hours. Within the freezing-tolerant bulk only, RNA was collected
311 from 6-week-old seedlings at control temperature (22°C) and after 7 days of cold acclimation
312 (5°C), with expression compared between these conditions (tol_5C vs. tol_22C). The second
313 transcriptome from *Tripsacum* 'Pete' (leaf, root, top-crown, and bottom-crown) was generated
314 using the same methodology (5°C vs. 22°C) as in Xue et al. (2021) and is currently
315 unpublished.

316 F_2 seedling leaf RNA was extracted following Gault et al. (2018). Paired-end reads were
317 quality-trimmed using Trimmomatic (v0.32; Bolger et al., 2014), aligned to the T. dactyloides
318 genome (Td-FL_9056069_6-DRAFT-PanAnd-1.0) using STAR v2.7.10b, and quantified with
319 featureCounts v2.0.3. Differential expression was assessed using DESeq2 (Love et al., 2014),
320 modeling temperature and genotype as main effects. Genes were considered differentially
321 expressed at adjusted $P < 0.05$ (Benjamini-Hochberg) and $|\log_2 FC| > 1$. Trimming parameters,
322 STAR alignment settings, and the full DESeq2 model are detailed in Methods S1.

323 *Structural and Biophysical Analysis of LEA3 Proteins*

324 Because LEA3 emerged as the only differentially abundant protein consistently elevated across
325 all five species (see Results) we performed targeted structural and biophysical analyses to
326 characterize its repeat architecture and cryoprotective potential. LEA3 orthologs from all five
327 study species plus *Zea mays* were aligned using MAFFT v7.520 with default settings.

328 Predicted three-dimensional structures for the *Tripsacum dactyloides*
329 (Td00001aa022594_T002) and *Zea mays* (Zm00001eb294480) orthologs were generated using
330 AlphaFold3 (Abramson et al., 2024) with default parameters and full length amino acid
331 sequence as input. Hydrophobicity was visualized in PyMOL (v2.5) using a custom script
332 based on the Eisenberg scale, which colored residues according to side-chain properties.
333 Hydropathy plots were generated using both ProtScale (ExPASy) and AmphipaSeek (Sapay et
334 al., 2006), with a sliding window size of 11 amino acids corresponding to the LEA3 motif
335 length. Hydrophobic peaks associated with conserved LEA motifs were annotated across both
336 sequence alignments and structural models.

Results

To examine seasonal proteomic responses in PACMAD grasses, we analyzed rhizome tissues of five species using a proteomic shotgun approach during the winter (January) and summer (August) of 2019-2020 and 2022 (Fig. 1) in Ithaca, New York (USDA Hardiness Zone 6a). The exposure to deep-freezing winters ensured that the proteomic responses captured were reflective of natural seasonal variation (Fig. 1b).

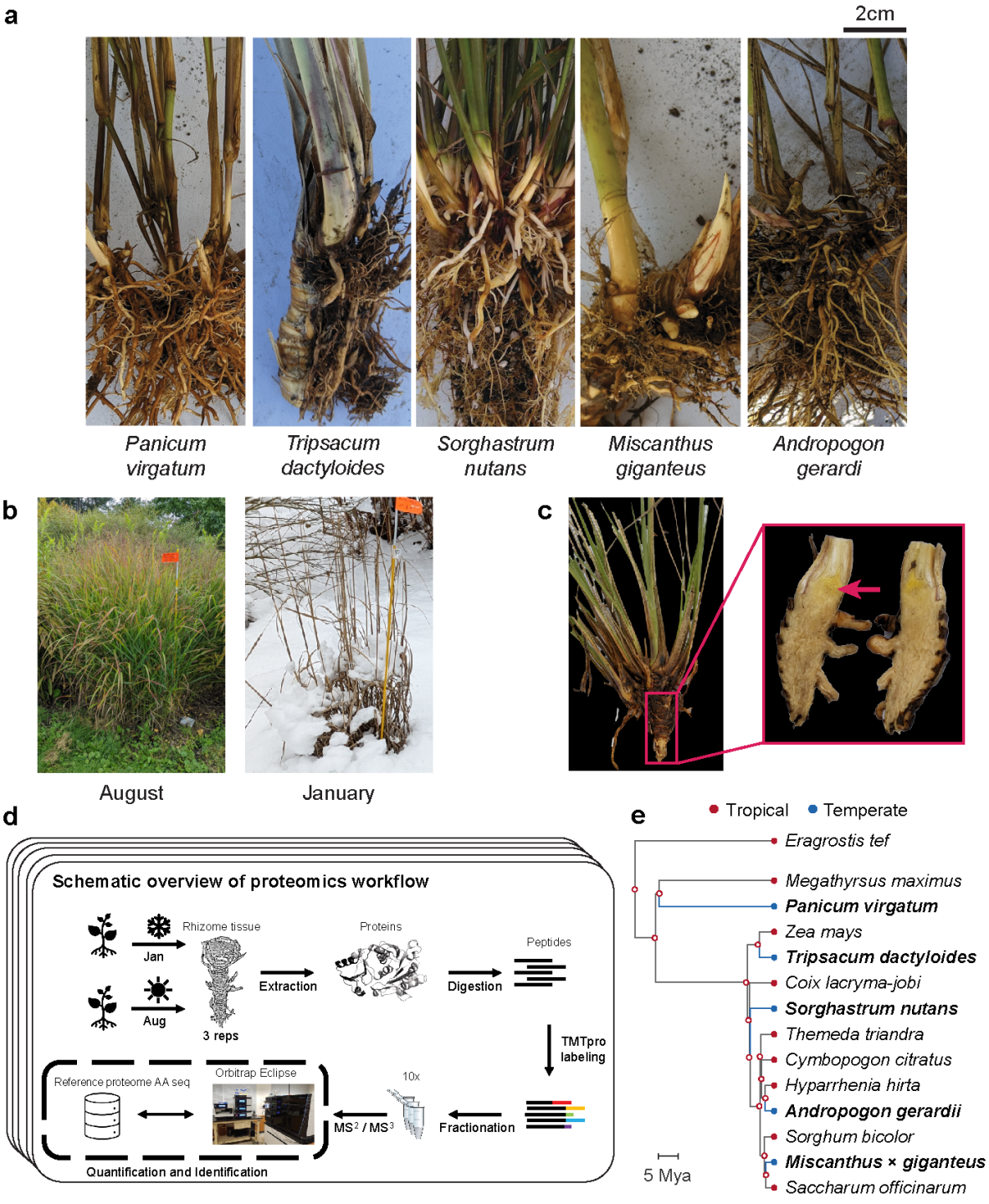

Fig. 1. Overview of sampling and proteomics workflow. (a) Rhizomes from the five species sampled in the study: *Tripsacum dactyloides* and *T. floridanum* hybrids, *Panicum virgatum*, *Andropogon gerardi*, *Miscanthus* × *giganteus*, and *Sorghastrum nutans*. **(b)** Field conditions during the two sampling seasons, illustrating the active growth in August and dormancy in January. **(c)** Example of the rhizome tissue sampled for proteomics, shown here for *Tripsacum*. The red arrow highlights the specific region collected. **(d)** Schematic overview of the proteomics workflow. Rhizome samples were collected each season, followed by protein extraction, digestion, and TMTpro labeling. Peptides were fractionated and analyzed via RTS-SPS-MS^3 using an Orbitrap Eclipse mass spectrometer. Each species' reference proteome was used for peptide and protein assignment, enabling quantification and identification. **(e)** Phylogenetic relationships among the five study species (bold) and tropical relatives, rooted on *Eragrostis tef* (Chloridoideae). Red, tropical; Blue, temperate and freezing tolerant.

355 Protein abundance analysis was performed in batches (see Methods). Across all five species a
356 total of 20,737 proteins were quantified, but for differential accumulation across seasons we
357 included only those quantified in both winter and summer samples (Table 1, Fig. S4). The
358 number of identified proteins ranged from 2,372 to 4,451 per species. Differentially abundant
359 proteins (DAPs) varied across species, with 58–174 proteins significantly increased and 56–
360 218 decreased in abundance under freezing conditions (Table 1). PCA of 745 shared
361 orthogroups confirmed clustering by species and season (Fig. S2); batch-corrected *Tripsacum*
362 samples (1,889 proteins) clustered by season regardless of hybrid background (Fig. S2b).
363 Although fewer proteins were identified in *Sorghastrum nutans*, reflecting its draft genome
364 status (Table S2), robust seasonal signatures were detectable across all five lineages (Fig. S2a).

365 **Table 1.** Summary of rhizome proteomics datasets for *Tripsacum* hybrids, *Andropogon gerardi*, *Miscanthus × giganteus*, *Panicum virgatum*, and *Sorghastrum*
366 *nutans*, including number of samples per season, total proteins quantified, proteins shared across seasons, and differentially accumulated proteins (DAPs)
367 accumulated (up) or depleted (down) in winter.

Species	Year	N samples	Genotype / Cultivar	Entry code	Clonal reps	Proteins quantified		DAP up	DAP down
						Total	Shared winter/summer		
Tripsacum spp.	2019	8	*T. dactyloides 'IA_Pete_2' × T. floridanum*	C002	1	4,451	4,451	123	175
			T. dactyloides 'KS_C9_9' × T. floridanum	C004	1				
			T. dactyloides 'KS_B6_1' × T. floridanum	C022	3				
			T. dactyloides 'KS_C9_10' × T. floridanum	C031	1				
			T. dactyloides 'IA_Pete_1' × T. dactyloides 'FL'	C071	1				
			T. dactyloides 'TX_HC_3' × T. dactyloides 'MO_TP'	C076	1				
Tripsacum spp.	2022	24	*T. dactyloides 'IA_Pete_2' × T. floridanum*	C002	3	3,468	3,054	100	141
			T. dactyloides 'KS_C9_9' × T. floridanum	C004	3				
			T. dactyloides 'KS_B6_1' × T. floridanum	C022	3				
			T. dactyloides 'KS_C7_3' × T. floridanum	C027	3				
			T. dactyloides 'IL_10_1' × T. floridanum	C043	3				
			T. dactyloides 'IL_14' × T. dactyloides 'FL'	C065	3				
			T. dactyloides 'IA_Pete_1' × T. dactyloides 'FL'	C071	3				
			T. dactyloides 'TX_HC_3' × T. dactyloides 'MO_TP'	C076	3				
Andropogon gerardi	2022	3	Sentinel	01-266*A	3	3,734	3,733	109	76
Miscanthus × giganteus	2022	3	-	88-363*A	3	2,372	2,273	58	83
Panicum virgatum	2022	3	Dust Devil	01-277*B	3	4,071	4,068	174	218
Sorghastrum nutans	2022	2	Golden Sunset	22-095*A	2	2,641	2,464	66	56

368

369 *Cross-Species comparative proteomic analysis reveals conserved seasonal protein*
370 *accumulation patterns*

371 We restricted our comparative analysis to the 18,454 proteins assigned to 4,888 orthogroups
372 identified across species (Tables S3 and S4). Seasonal fold-changes were positively correlated
373 across all species pairs (ρ = 0.37-0.69; Fig. 2a), with specific orthogroups—including LEA3,
374 GST, HSP1, and PEBP—consistently identified as differentially abundant. To test whether this
375 conservation reflects evolutionary constraint on cold response, we compared fold-change
376 correlations between shared DAPs (differential abundance in ≥2 species; n = 135 orthogroups)
377 and background proteins (≤1 species; n = 1,548). Shared DAPs showed substantially higher
378 correlation in seasonal response magnitude (ρ = 0.80) than background (ρ = 0.45; $P = 1.1\times10^{-5}$;
379 Fig. 2b). Notably, this constraint did not extend to basal abundance, where shared DAPs
380 showed slightly lower correlation than background (ρ = 0.62 vs 0.68; P = 0.004). This pattern—
381 tight constraint on response dynamics but flexibility in baseline levels—suggests that
382 independent cold adaptations are governed by conserved regulation of a core set of protective
383 proteins. This result was robust to the exclusion of *S. nutans*, which had fewer biological
384 replicates (n = 2 per season; P = 0.002).

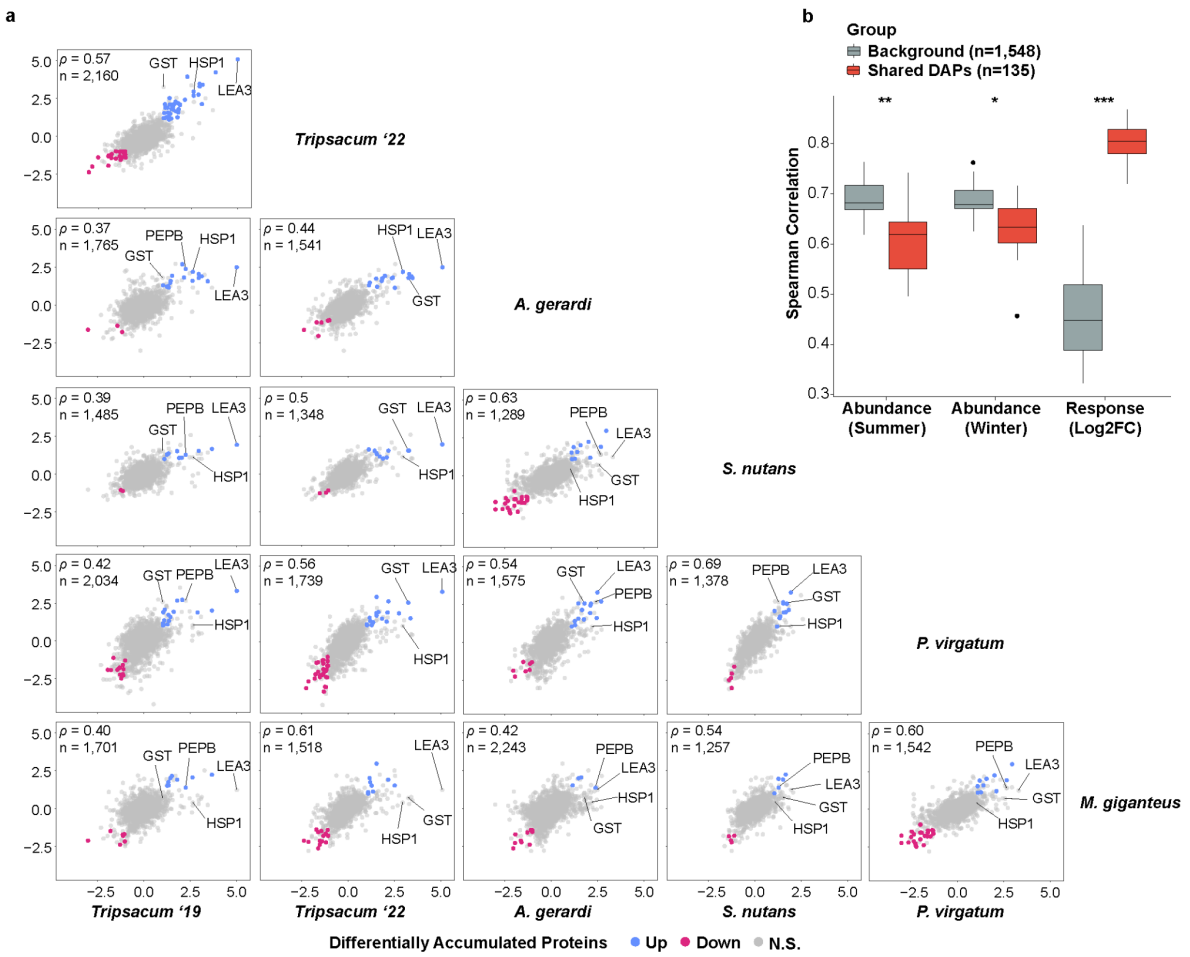

Fig. 2. Conservation of seasonal protein accumulation in rhizomes of *Tripsacum dactyloides* and *T. floridanum* hybrids, *Andropogon gerardi*, *Miscanthus* × *giganteus*, *Panicum virgatum*, and *Sorghastrum nutans*. (a) Pairwise comparisons of $\log_2$ fold-change ($\log_2$FC winter/summer) in differentially accumulated orthogroups across species. Scatterplots display the correlation of orthogroup-level $\log_2$FC values between species, with shared DAPs elevated in winter shown in blue, reduced in red, and non-significant proteins in gray. Each panel represents a comparison between two species, with the number of shared orthogroups (*n*) and Spearman's correlation coefficient (ρ) displayed. **(b)** Pairwise Spearman correlations for orthogroups quantified in at least four of five species, comparing shared DAPs (red; differentially abundant in ≥2 species) versus background orthogroups (gray; differentially abundant in ≤1 species). Correlations are shown for summer abundance, winter abundance, and seasonal response magnitude ($\log_2$FC winter/summer). Wilcoxon rank-sum test: *P < 0.05, **P < 0.01, ***P < 0.001.

Ortholog and pathway sharing across species

We next examined orthogroup sharing across species (Fig. S5). Winter-elevated orthogroups showed greater conservation than winter-reduced: 27% of 330 winter-elevated orthogroups were shared across at least two species versus 21% of 470 winter-reduced orthogroups.

403 Variation in identified proteins partly reflects reference proteome completeness—*S. nutans*,
404 with a draft genome containing 26% ambiguous bases, yielded fewer identifications (Table
405 S2).

406 GO enrichment analysis revealed distinct functional signatures (Fig. S6a). Winter-elevated
407 proteins were enriched for protein folding, stress response, cold acclimation, and ROS
408 scavenging (Table S5). Winter-reduced proteins were enriched for microtubule-based
409 processes, mitotic cell cycle, cytoskeleton organization, and cell wall biogenesis—processes
410 associated with active growth (Table S6). The greater conservation of winter-elevated
411 orthogroups suggests that protective responses to freezing are more constrained than growth-
412 related processes active during summer. To identify the most conserved functional themes, we
413 examined the 50 most winter-elevated proteins per species (Fig. 3; Table S7). LEAs and heat
414 shock proteins (HSPs) were present in at least four of five species. A chi-square test on standard
415 GO categories revealed significant species heterogeneity ($\chi^2[70] = 97.5$, $P = 0.017$), but GO
416 terms may conflate cold-specific processes with broader stress responses (Barnes et al., 2023).
417 63% of proteins mapped to one of nine functional groups curated for relevance to cold (Fig.
418 S6b). Heterogeneity remained significant ($\chi^2[40] = 58.1$, $P = 0.032$; Fig. 3a), indicating that
419 while species share the same core functional categories, they differ in relative investment.
420 Detoxification and ROS scavenging proteins were represented in all five species.
421 Metabolism/osmoregulation proteins were less prominent in *A. gerardi*, while protein
422 aggregation and membrane stability proteins were enriched in *A. gerardi* and *P. virgatum*.
423 These patterns indicate a shared functional core with lineage-specific variation in relative
424 allocation (Fig. 3a), particularly in metabolism/osmoregulation and protein folding/stability.

425 LEA3 (OG0022470) was the only ortholog ranked among the top 10 winter-elevated proteins
426 in all five species and was the single most elevated protein in *Tripsacum* ($\log_2$FC = 5.0; Fig.

427 3b; Table S7). Other functional categories showed species-specific representation: HSPs
428 appeared in the top 10 for *Tripsacum* (HSP22, Class IV) and *S. nutans* (HSP23.2) but involved
429 different family members; ROS scavenging was universal but employed glutathione
430 transferases in four species and peroxidases in *A. gerardi*; putative antifreeze proteins
431 (chitinases) ranked highly in *S. nutans* and *A. gerardi*. This pattern—a single conserved
432 ortholog (LEA3) alongside functionally equivalent but distinct proteins in other categories—
433 exemplifies parallel recruitment of LEA3 alongside functional convergence for chaperone and
434 antioxidant functions.

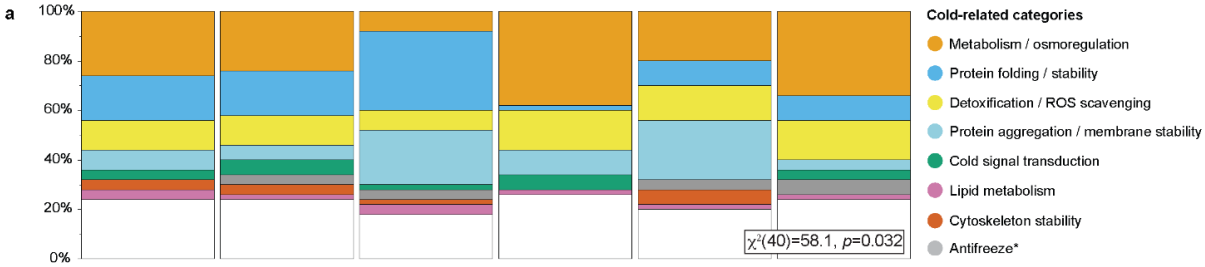

b

Rank	*Tripsacum* 2019	*Tripsacum* 2022	*A. gerardi*	*M. giganteus*	*P. virgatum*	*S. nutans*
1	LEA3	LEA3	PEBP	NDUFS1	Embryonic DC-8	Barwin
2	HSP22.0	Abscisic stress ripening	Chitinase	Embryonic DC-8	LEA3	Zeamatin
3	Abscisic stress ripening	Uncharacterized	Actin-depolymerizing 2	Malate synthase	Isoflavone hydroxylase	LEA3
4	TLC	HSP, chloroplastic	Subtilisin-chymotrypsin	Aldose reductase	PEBP	Chitinase
5	Aldose reductase	HSP22.0	LEA-D34	Uncharacterized	Dehydrin	Uncharacterized
6	Dehydrin	HSP I	LEA3	UDP-glucose epimerase	LEA-D34	Chitinase
7	SBP65	WIBG Mago-binding	LEA3	LEA3	LEA3	LTI65
8	PG inhibitor	Chitinase	Uncharacterized	TIF3 subunit G	NDUFS1	UDP-glucose epimerase
9	HSP, chloroplastic	EFHD	Uncharacterized	HSP70 BIP2	LEA14-A	Aldose reductase
10	Dehydrin	HSP16.9A	HSP I	Beta-amylase	Actin-depolymerizing 3	ATP-PFK 2
11	EFHD	Aldose reductase	HSP I	Aldose reductase	GEM-like protein 5	Protein IN2-1
12	GST	HSP70	LEA3	LEA-D34	GST	OEP162
13	Methionine γ-lyase	OEP162	GH18	Reticulon-like	Nematode HSPRO2	Tryptophan synthase
14	OEP162	Dehydrin	HSP I	GEM-like protein 5	Uncharacterized	EFHD
15	DOL monooxygenase	TIL1	HSP I	Ureidoglycolate hydr	Xylanase inhibitor	GST
16	Dehydrin	Chitinase	LTI65	Tryptophan synthase	LTI65	GEM-like protein 5
17	TIL1	Cylicin-1	Ribonuclease 1	PEBP	Actin-depolymerizing 3	HSA32
18	UDP-glucose epimerase	TSJT1	HSP I	Raffinose synthase	LTI65	Anthranilate PRTase
19	HSP16.9A	Uncharacterized	Embryonic DC-8	LTI65	GEM-like protein 5	TVP15
20	1,3-Beta-glucosidase	Aconitase 1	LTI65	Pathogenesis-related 1	Chitinase	Ca-transporting ATPase
21	sHSP17.8	HSP I	HSP, mitochondrial	LEA14-A	GST	Anthranilate PRTase
22	Nitrite reductase	Starch synthase	HSP23.2	PV42a	Embryonic DC-8	Phosphoglycerate mut
23	GST	Malate synthase	LTI65	Tryptophan synthase	OPR1	AAA+ ATPase
24	Transmembrane protein	Heme-binding protein	rRNA N-glycosylase	Peroxidase	UMP-CMP kinase	HSP70 8
25	PEBP	sHSP17.8	EFHD	Tryptophan synthase	SBE II-1	PEBP
26	Aconitase 1	PEP carboxykinase 2	Phosphoglycerate mut	GLO3	HSP70	Reticulon-like
27	KOW	GEM-like protein 5	PEBP	Senescence domain	Pre-mRNA-processing	Phosphoglycerate mut
28	Malic enzyme	Protein DETOX	sHSP26	TSJT1	Embryonic DC-8	DUF255
29	HSP I	UspA	Uncharacterized	GST	GST	Transketolase
30	Actin-depolymerizing 3	sHSP17.8	Pyruvate decarboxylase	Aminotransferase III	Phosphoglycerate mut	AGPase
31	Fe2OG dioxygenase	Cylicin-1	protein-di-S reductase	14-3-3 protein 7	Dehydrin	HSP I
32	Protein DETOX	UspA	Ricin	Ricin B-like lectin	HSP III	Alcohol dehydrogenase
33	sHSP17.8	cpRBP	Peroxidase	DUF255	Aldose reductase	PDH-E1α
34	PEP carboxykinase 2	Fe2OG dioxygenase	Dirigent protein	Anthranilate synthase	OEP162	DJ-1/Pfpl
35	UspA	Sucrose synthase	HSP70	AAA+ ATPase	FAD-binding PCMH	HSP II
36	HSP70	Starch synthase	HSP83	DJ-1 homolog B	HSP70	UspA
37	Starch synthase	Beta-glucosidase 31	LEA-D34	OEP162	LEA-D34	GST
38	GST	Dipeptidylpeptidase IV	LEA-D34	Thiamine thiazole	MORF2	Cystatin-1
39	sHSP17.8	Malic enzyme	Dirigent protein	GPT2	HSP, mitochondrial	Cystatin-1
40	GEM-like protein 5	GST	Thioredoxin	Ca-transporting ATPase	Cylicin-1	Dipeptidylpeptidase IV
41	Phloem-specific lectin	Peroxidase	Peroxidase	Peptidase M48	VOC	TATA-binding protein
42	Cylicin-1	Starch synthase	Aconitase 1	Pectinesterase inhibitor	HSP101	AGPase
43	GNAT family	AGPase	Malic enzyme	Pre-mRNA-processing	OEP162	ClpB2, chloroplastic
44	Cytochrome P450	RAB5	Zeamatin	14-3-3 protein 7	ATP-PFK 2	GST
45	Starch synthase	LEA-D34	HSP23.2	DJ-1 homolog D	AAA+ ATPase	CYFBP
46	Starch synthase	Abscisic stress ripening	Aldose reductase	Anthranilate PRTase	SBE II-1	Tryptophan synthase
47	W2	HSP70 8	sHSP26	Galactokinase	Malic enzyme	Zinc-regulated GTPase
48	HSP83	Acyl transferase 5	Embryonic DC-8	GST	Phosphoglycerate K	Dienelactone hydrolase
49	Adenylate kinase	Cytochrome P450	HSP70	PDH-E1α	Chitinase	Malic enzyme
50	IPS3	GST-N	sHSP	GLO3	PCYOX	Peroxidase

Fig. 3. Overview of cold-related functional categories represented among the top 50 most winter-enriched rhizome proteins *Tripsacum dactyloides* and *T. floridanum* hybrids, *Andropogon gerardi*,

***Miscanthus* × *giganteus*, *Panicum virgatum*, and *Sorghastrum nutans*. (a)** Mosaic plot of cold-related functional categories across species. This plot visualizes the distribution of proteins among cold-related functional categories for each species. The relative abundance of each category within a species is shown, highlighting distinct functional profiles and species-specific variations in cold tolerance mechanisms. A Chi-square test for independence ($\chi^2[40] = 58.1$, $P = 0.032$) was performed to evaluate variation across species. **(b)** Visual representation of cold-related functional categories in rhizome proteins of five *Andropogoneae* species. This figure illustrates the top 50 most abundant proteins within the rhizomes of five *Andropogoneae* species. Proteins are classified into functional categories relevant to cold-related mechanisms, such as metabolism/osmoregulation, cold signal transduction, membrane stability, lipid metabolism, and others. Color-coding facilitates a comparative visualization of cold tolerance mechanisms across species. Antifreeze proteins are marked by an asterisk, as their classification is based solely on protein homology.

Evolutionary patterns in accumulated protein families

Phylogenetic analysis revealed distinct evolutionary patterns between LEAs and HSP families (Fig. 4). The control elongation factor 1 protein (EF1) family, previously shown to have stable expression at transcript and protein levels across conditions (Takamori et al., 2017, Fig. 4a), showed minimal seasonal accumulation and no phylogenetic clustering of abundance level patterns, consistent with their housekeeping function (Table S8). HSPs showed greater diversity (212 proteins across 37 orthogroups, Table S9) compared to LEAs (66 proteins in 20 orthogroups, Table S10), with control EF1 comprising 33 proteins in 4 orthogroups. Both LEA and HSP phylogeny (Figs. 4b and c) resolved into clear functional sub-families, but among HSPs the most strongly winter-elevated members ($\log_2FC > 2.5$) belonged to different clades across different species, with only 32% of HSP proteins significantly elevated in winter. In contrast, LEA proteins (Fig. 4b) demonstrated more consistent winter abundance (47% of the proteins), particularly within the LEA3 subfamily, which displayed elevated abundance across all species despite having diverged earlier than other LEA clades.

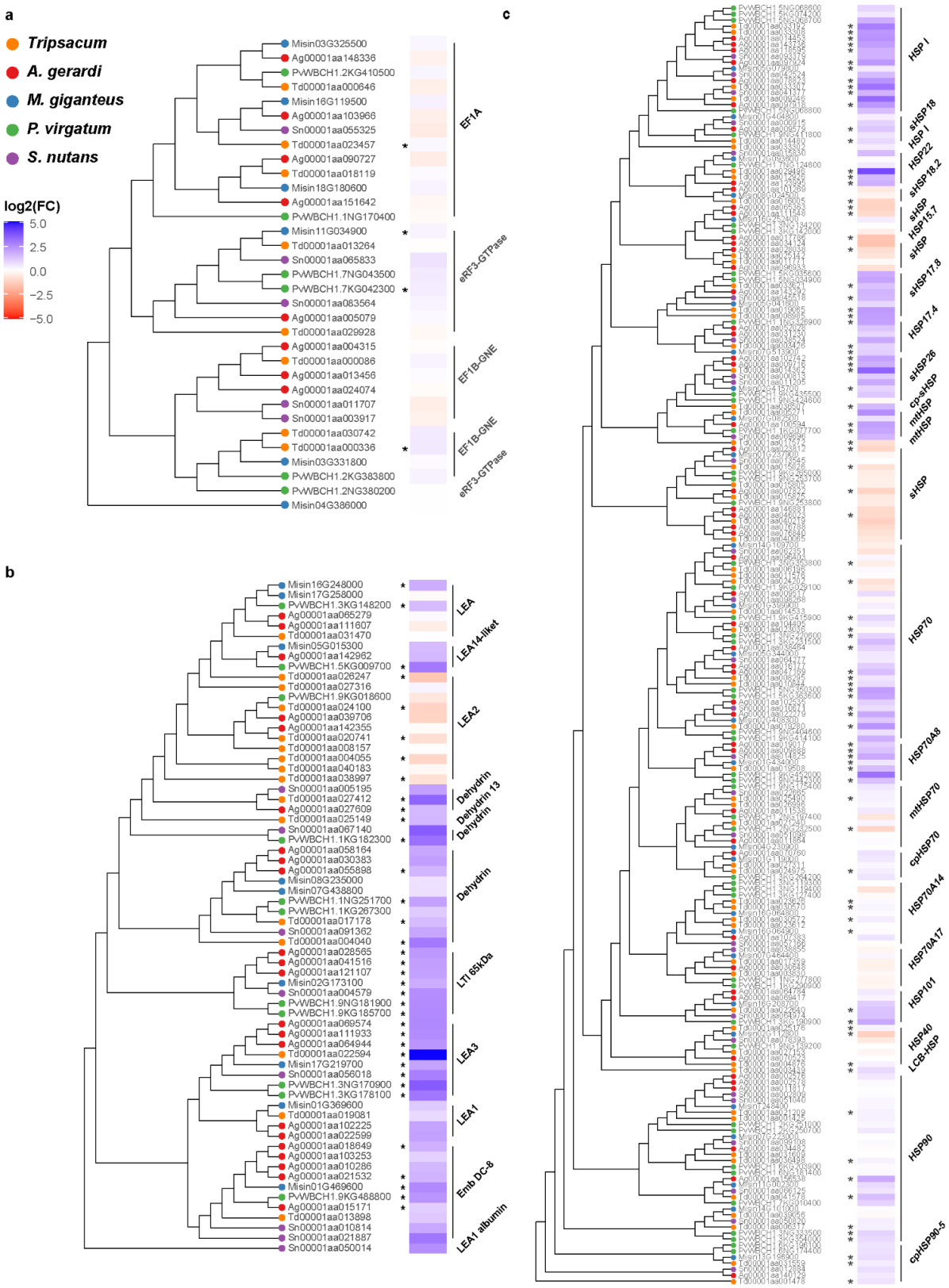

465

466 **Fig. 4. Phylogenetic analysis and seasonal abundance dynamics of selected protein families across**
467 ***Tripsacum dactyloides* and *T. floridanum* hybrids, *Panicum virgatum*, *Andropogon gerardi*,**
468 ***Miscanthus* × *giganteus*, and *Sorghastrum nutans*.** Protein identifiers represent species-specific
469 sequences, and brackets denote functional group annotations, merging adjacent orthogroups with

470 similar functions for clarity. Heat maps illustrate $\log_2$ fold-change ($\log_2$FC) in protein abundance
471 between winter and summer conditions, where blue indicates higher abundance in winter, and red
472 signifies higher summer abundance. Panels show distinct protein families: **(a)** translation elongation
473 factor 1 proteins (EF1; control group) , **(b)** late embryogenesis abundant (LEA) proteins, and **(c)** heat
474 shock proteins (HSPs). Asterisks (*) mark proteins exhibiting statistically significant differential
475 accumulation ($P < 0.05$).

476 *Beyond rhizomes: Comparison with maize & Tripsacum mRNA*

477 We next tested whether rhizome protein signatures corresponded to mRNA responses in other
478 tissues. Cold-induced mRNA in F_2 seedling leaves of *Tripsacum*, derived from the same
479 hybrids used in our rhizome study, showed weak but significant correlation with rhizome
480 protein fold-changes ($\rho = 0.29$, $P < 0.001$; Fig. S7a). Other *Tripsacum* tissues showed weaker
481 correlations ($\rho = 0.08$–0.16; Fig. S7b–e), as did maize orthologs ($\rho = 0.01$–0.09; Figs. S7f–i).
482 Despite these weak overall correlations, LEA3 displayed strong cold induction in leaves of
483 both species ($\log_2$FC = 8 in *Tripsacum*, and 7 in maize; Fig. S7a and f). That maize induces
484 LEA3 transcription to levels comparable to cold-tolerant *Tripsacum*, yet remains freezing-
485 sensitive, suggests that transcriptional induction of *LEA3* alone does not confer protection.

486 *Structural and Functional Insights into LEA3: A Key Player in Freezing Tolerance*

487 LEA3 (OG0022470) was the only ortholog consistently elevated across all five species, ranking
488 as the top DAP in *Tripsacum* rhizomes ($\log_2$FC = 5.0) and the most cold-induced transcript in
489 leaves ($\log_2$FC = 8). Sequence alignment revealed that all six PACMAD orthologs share the
490 Group 3 LEA architecture (Fig. S8), featuring tandem 11-mer repeats that fold into amphipathic
491 α-helices (Fig. 5b). LEA3 proteins are classified as intrinsically disordered proteins thought to
492 adopt amphipathic alpha-helical conformations upon binding to membranes or other proteins
493 during cellular dehydration (Kovacs et al. 2008). These repeats generate characteristic
494 oscillations in Kyte-Doolittle hydropathy profiles (Fig. 5c; Table S11; Fig. S9), consistent with
495 a hydrophobic face (positions 1, 2, 5, 9) and a charged hydrophilic face essential for desiccation
496 and freezing tolerance (Dure, 1993). While the number of repeats varied—ranging from three

497 (*M. giganteus*, *Z. mays*) to five (*T. dactyloides*, *A. gerardi*)—total LEA3 dosage was further
498 modulated by gene copy number, with *A. gerardi* and *P. virgatum* accumulating multiple
499 paralogs (Fig. 4b; Table S12). Notably, although *M. giganteus* and *Z. mays* share the same
500 three-repeat architecture, their biophysical properties diverge. The *M. giganteus* ortholog
501 retains hydrophilic consensus repeats, while the maize ortholog contains a variant third repeat
502 (`AADAMEAAKQK`) with alanine and methionine substitutions that increase local hydrophobicity
503 (repeat GRAVY −0.67 vs consensus mean −1.41; Table S12). This variation produces a distinct
504 hydrophobic peak in the hydropathy profile (Fig. 5c) and a more pronounced hydrophobic face
505 in the predicted structure (Fig. 5b), potentially compromising the balance between hydrophobic
506 and hydrophilic faces required for effective cryoprotection. Hydrophobicity scores for
507 individual LEA3 orthologs are provided in Table S11.

508 Hydropathy profiles from all cold-tolerant species examined show oscillating patterns
509 consistent with amphipathic helix periodicity (Fig. S9). Species with more repeats exhibit more
510 oscillation cycles and consequently longer amphipathic regions. Outgroup LEA3 proteins from
511 wheat (TdLEA3; Koubaa et al., 2019) and *Arabidopsis* (AtLEA7; Popova et al., 2015) showed
512 comparable repeat architecture. These observations suggest that transcriptional induction of
513 *LEA3* alone may not ensure freezing tolerance and that functional protection may depend on
514 both protein accumulation in the appropriate tissue and the biophysical properties of the tandem
515 repeats of the 11-mer motif.

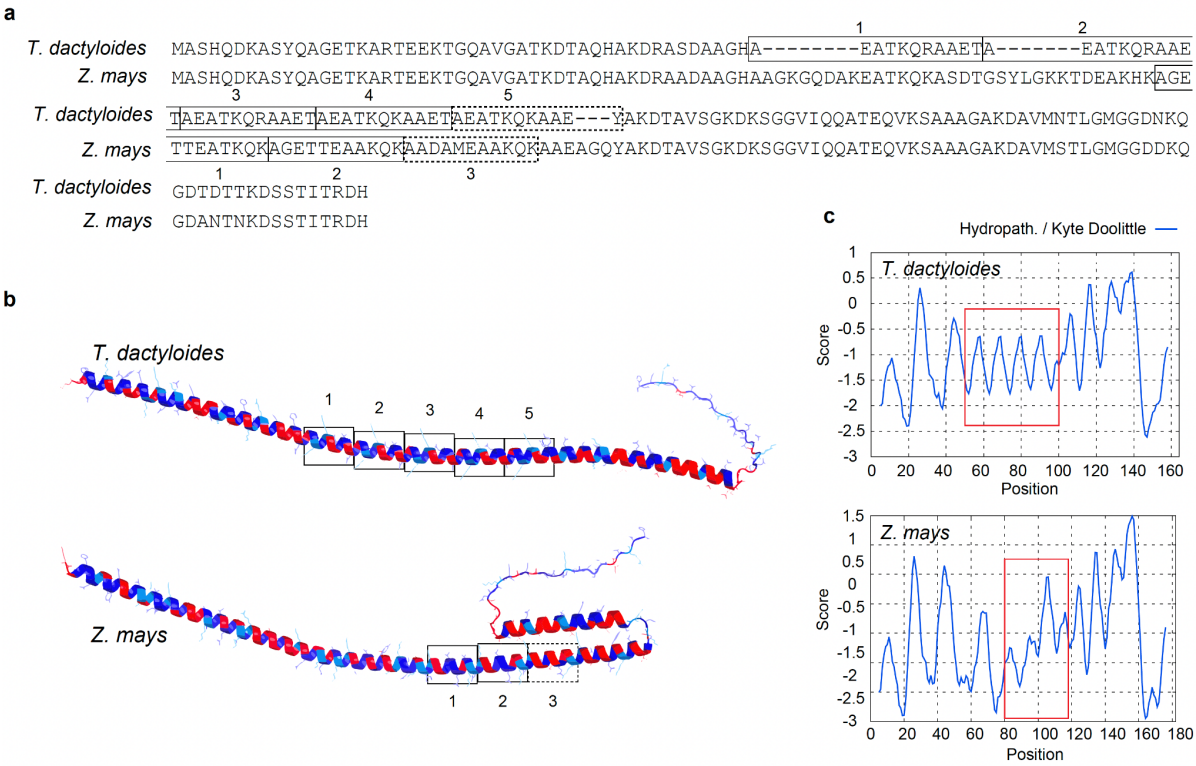

Fig. 5. Protein sequence alignment, structure and hydrophobicity of LEA3 orthologs from *Tripsacum dactyloides* and *Zea mays*. (a) The alignment shows the LEA3 proteins from *T. dactyloides* (Td00001aa022594_T002) and, *Z. mays* (Zm00001eb294480), with tandem 11-mer repeat units highlighted and labeled numerically. *T. dactyloides* contains five repeat units (1–5); *Z. mays* contains three (1–3). The dashed box indicates a repeat unit with variant residues relative to the consensus repeat sequence. (**b**) Predicted secondary structure of LEA3 proteins using AlphaFold3, showing the conserved alpha-helical domains across *T. dactyloides* (top) and *Z. mays* (bottom). Repeat regions corresponding to labeled sequence motifs are boxed. Red and blue indicate regions of high hydrophilicity and hydrophobicity, respectively. **(c)** Kyte-Doolittle hydropathy plots for LEA3 proteins. The X-axis represents residue position, while the Y-axis indicates hydropathicity scores (positive values for hydrophobic regions, negative for hydrophilic regions). Red boxes highlight the amphipathic region encompassing the 11-mer tandem repeat array, corresponding to key domains in (b)**.**

Discussion

Our analysis of rhizome proteomes from five independently cold-adapted PACMAD grasses reveals that protein-level cold responses combine ancestral retention of core protective orthologs with convergent deployment of functionally equivalent but phylogenetically distinct proteins. The clearest example of retention is LEA3, accumulated across all five lineages: its early divergence from other LEA subfamilies (Fig. 4b) and the conservation of its tandem 11-mer repeat architecture across cold-tolerant species suggest that the cryoprotective capacity of

537 LEA3 predates the PACMAD radiation and has been maintained under constraint in lineages
538 that colonized cold environments (Fig. 1e). In contrast, the chaperone response illustrates
539 convergent evolution: different HSP family members are recruited in different species,
540 suggesting that chaperone-mediated protection permits greater flexibility in which family
541 members are deployed. To our knowledge, this study provides the first quantitative comparison
542 of cross-species fold-change conservation at the protein level in a freezing-stress context,
543 complementing transcript-level comparisons in *Pooideae* (Schubert et al., 2019) and
544 desiccation-tolerance studies in resurrection grasses (Marks et al., 2024).

545 The most striking finding is the evolutionary constraint on response magnitude. Among shared
546 cold-responsive orthogroups, cross-species fold-change correlations were substantially higher
547 (ρ = 0.80, Fig. 2b) than among background proteins (ρ = 0.45; P = 1.1 × 10^{-5}), indicating that
548 when freezing tolerance evolved independently across PACMAD lineages, it proceeded
549 through quantitatively similar responses in a core set of protective proteins. Our common-
550 garden design ensured identical winter conditions across all genotypes, with winter collections
551 following sustained sub-zero exposure reaching −16°C and soil temperatures below 2–5°C for
552 20–22 days (Brotzge et al., 2020), while summer collections captured vigorous growth with
553 actively emerging rhizome buds after >90 mm cumulative precipitation (Fig. S1), establishing
554 these seasonal contrasts as cold-driven rather than drought-related. A limitation of this design
555 is that all species experienced identical winter conditions rather than stress calibrated to each
556 species' tolerance threshold.

557 With these responses established as cold-driven, their conservation contrasts sharply with
558 transcript-level patterns: comparative transcriptomics in *Pooideae* found generally low
559 similarity in cold-responsive gene expression across species (r = 0.09–0.40; Schubert et al.,
560 2019), with nearly half of all cold-responsive genes being species-specific. This comparison

561 spans different clades, tissues, and experimental designs — our PACMAD rhizome proteomes
562 versus *Pooideae* seedling transcriptomes — so the gap between protein-level and transcript-
563 level correlations may be confounded by these differences. Nevertheless, the direction is
564 consistent with the framework of Cope et al. (2025), who demonstrated that protein abundances
565 are under stronger stabilizing selection than mRNA abundances over macroevolutionary
566 timescales, with mutations affecting mRNA levels largely buffered before they alter protein
567 output. If this buffering operates on cold-responsive genes as it does genome-wide, then
568 transcript-level comparisons would systematically underestimate the degree of evolutionary
569 conservation in stress responses. Notably, this constraint applies specifically to the dynamic
570 response: absolute abundance correlations for shared cold-responsive proteins were lower than
571 background in both summer (ρ = 0.62 vs 0.68; P = 0.004) and winter (Fig. 2b), indicating that
572 these proteins are more divergent across species in their resting and stress-state levels. What is
573 conserved is not the absolute abundance in either season, but the magnitude of accumulation
574 when freezing arrives. This divergence in absolute levels likely reflects the distinct
575 physiological contexts of each species' rhizomes, including differences in dormancy depth,
576 metabolic rate, or tissue composition, while the conserved fold-change suggests that selection
577 acts primarily on the dynamic response rather than on any single optimal protein concentration.

578 LEA3 provides the clearest illustration of this constraint and connects the evolutionary pattern
579 to a mechanistic hypothesis. LEA proteins function as molecular shields during freezing
580 through membrane stabilization, the prevention of protein aggregation, and the protection of
581 client proteins through steric exclusion and stress induced conformational changes (Kovacs et
582 al., 2008; Cuevas-Velazquez et al., 2017). These functions depend on the repeating 11-mer
583 motif architecture, described by Dure (1993), in which apolar residues form the hydrophobic
584 face of α-helices that bind membranes and partially unfolded proteins during dehydration and
585 freezing (Koubaa *et al.*, 2019; Singh & Graether, 2021).

586 The structural data support a model in which cryoprotective efficacy arises from three factors:
587 amphipathic helix length per protein (determined by repeat number), total protein abundance
588 (increased through paralog accumulation in *A. gerardi* and *P. virgatum*), and repeat
589 composition. All cold-tolerant species and outgroups maintain conserved amphipathic
590 character across their 11-mer repeats (Figs. S8, S9; Table S12), whereas the variant third repeat
591 of Z. mays shows an exaggerated hydrophobic face that may compromise the amphipathic
592 balance required for effective cryoprotection (Table S12). AlphaFold3 multimer predictions
593 reinforce this distinction: while both Td and ZmLEA3 form tetrameric assemblies, they adopt
594 distinct packing geometries (Fig. S10), consistent with observations that cereal LEA3 proteins
595 require conserved domains for oligomerization (NDong *et al.*, 2002) and Arabidopsis LEA3
596 proteins form higher-order assemblies under stress (Ginsawaeng et al., 2021; Romero-Pérez et
597 al., 2024). The variant hydrophobic face in ZmLEA3 may disrupt the optimal packing
598 arrangement required for effective cryoprotection. This structural divergence helps explain
599 why, although ZmLEA3 is cold-inducible and confers partial cold tolerance (Liu et al., 2013),
600 maize remains freezing-sensitive despite accumulating transcripts to levels comparable to the
601 cold-tolerant *Tripsacum* in leaves (Fig. S7f). Transcriptional induction alone does not ensure
602 protection; functional efficacy depends on both sufficient abundance and activity, the latter
603 shaped by the biophysical properties of the repeat region. The early divergence of LEA3 from
604 other LEA subfamilies (Fig. 4b) suggests that the molecular properties enabling cryoprotection
605 were likely present before the PACMAD radiation. Cold-tolerant lineages maintained or
606 expanded LEA3 repeat number and in some cases accumulated multiple paralogs, while in
607 maize — where freezing selection was relaxed — repeat number was not expanded and the
608 third repeat diverged from the hydrophilic consensus.

609 Yet, freezing survival involves the coordinated action of numerous protective mechanisms, and
610 restoring a single protein's architecture in a freezing-sensitive species would be unlikely to

611 confer full tolerance. Rather, LEA3 illustrates how structural constraints at the protein level
612 could limit the efficacy of otherwise conserved transcriptional responses.

613 More broadly, several of the most consistently accumulated proteins across PACMAD
614 rhizomes have well-characterized orthologs implicated in cold acclimation in *Arabidopsis*,
615 including LEA proteins, small HSPs, and glutathione S-transferases (Marrs, 1996; Sun et al.,
616 2002; Hundertmark & Hincha, 2008), indicating deep conservation of core protective pathways
617 across monocots and dicots. However, some highly accumulated proteins in PACMAD
618 rhizomes—notably PEBP family members and certain chitinase-like proteins—have not been
619 prominently featured in *Arabidopsis* cold studies, potentially reflecting grass-specific or
620 rhizome-specific adaptations (Roeder et al., 2025).

621 The presence of ABA-inducible proteins and dehydrins among the most accumulated winter
622 proteins across species is consistent with shared physiological pathways between drought and
623 frost responses. While evidence shows that drought tolerance evolved before frost tolerance in
624 PACMAD grasses, suggesting they may have been co-opted, the extent to which this actually
625 happened remains unclear (Schat et al., 2025). In contrast, Pooideae grasses show a different
626 trajectory, where frost tolerance appears to have evolved independently of, or even prior to,
627 drought tolerance (Stolsmo et al., 2024; Schat et al., 2025).

628 In conclusion, rhizome freezing tolerance across independently cold-adapted PACMAD
629 grasses is governed by the retention of ancestral protective proteins under quantitative
630 constraint on response magnitude, combined with convergent deployment of diverse protein
631 families for chaperone and antioxidant functions. This constraint is substantially stronger at the
632 protein level than previously observed at the transcript level. The differences in LEA3 repeat
633 number and composition between cold-tolerant PACMAD species and maize offer a candidate
634 mechanism for enhancing freezing resilience in maize. Future work should prioritize functional

635 validation of LEA3 repeat variants, particularly testing whether restoring the ancestral
636 hydrophilic consensus or introducing additional paralogs can enhance frost tolerance in maize.

637 **Acknowledgments**

638 We thank Cornell Botanic Gardens for their support of this study and for maintaining the field
639 plots that provided essential plant material, particularly Kristine Boys, Emily Detrick
640 (Elizabeth Weaver Director of Horticulture), and Todd Bittner (Director of Natural Areas). We
641 acknowledge the Proteomics and Metabolomics Facility at the Cornell Institute of
642 Biotechnology (RRID:SCR_021743) for providing mass spectrometry services and data
643 analysis. We are grateful to Prof. Hening Lin for funding support from the HHMI
644 Transformative Technology 2019 program for the Orbitrap Eclipse system, and to Dr. Sheng
645 Zhang for NIH SIG grant support (1S10 OD017992-01 for the Orbitrap Fusion mass
646 spectrometer and 1S10 RR025449-01 for the Orbitrap Velos/Elite mass spectrometer). We
647 extend our appreciation to Elizabeth T. Anderson and Robert W. Sherwood at the Proteomics
648 and Metabolomics Facility for their technical expertise and assistance with sample processing
649 and analysis. We thank the Genomics Facility (RRID:SCR_021727) of the Biotechnology
650 Resource Center at the Cornell Institute of Biotechnology for their assistance with sequencing
651 experiments. Additional computational resources and data management were provided by the
652 Bioinformatics Facility (RRID:SCR_021757) at the Cornell Institute of Biotechnology. This
653 research is made possible by the New York State (NYS) Mesonet. Original funding for the
654 NYS Mesonet (NYSM) buildup was provided by the Federal Emergency Management Agency
655 grant FEMA-4085-DR-NY. The continued operation and maintenance of the NYSM is
656 supported by the National Mesonet Program, University at Albany, Federal and private grants,
657 and others. We acknowledge all who have contributed to the preservation, cultivation and study
658 of wild and domesticated grasses.

Competing interests

The authors declare no competing interests.

Author Contributions

M.C.R., T.E.R., and E.O. conceived and designed the study. N.L. and T.E.R. developed the long-term sampling strategy that enabled seasonal comparisons. N.L., T.E.R., T.L., S.-K.H., C.M.G., and E.O. performed sample collection and experimental work. T.L., R.A., and Q.F. conducted proteomics sample preparation, LC-MS/MS, and data processing. C.M.G., J.H., T.L., and J.Z. performed RNA-seq analysis. J.Z., S.-K.H., and E.O. carried out bioinformatics and statistical analysis. J.Z., S.-K.H., C.O.H., and E.O. prepared the figures. E.O., J.Z., L.J.B., and E.S.B. wrote the manuscript. C.O.H., L.J.B., S.-K.H., J.H., Q.F., E.S.B., and M.C.R. reviewed and edited the manuscript. E.O. and M.C.R. supervised the project and E.S.B. and M.C.R. acquired funding.

Funding

This research was supported by the National Science Foundation under Grant Number 1822330, and the U.S. Department of Agriculture–Agricultural Research Service (USDA-ARS) under Project Number 5030-21000-072-00-D (Corn Insects and Crop Genetics Research Unit, Ames, Iowa), Project Number 6066-21310-005-00-D (Genomics and Bioinformatics Research Unit, Stoneville, MS), Project Number 8062-21000-043-00-D (Plant, Soil and Nutrition Research Unit, Ithaca, NY), and the United States - Israel Binational Agricultural Research and Development Fund, Vaadia-BARD Postdoctoral Fellowship Award No. FI-628-2022. C.M.G. was supported by the National Science Foundation Postdoctoral Research Fellowship in Biology under Grant No. 1523861. Research in the lab of J.H. is supported by

USDA NIFA (2022-67013-37040). Q.F. was supported by HHMI Transformative Technology 2019 program for the Orbitrap Eclipse system.

Data Availability

The mass spectrometry proteomics data have been deposited to the ProteomeXchange Consortium via the PRIDE (Perez-Riverol et al., 2025) partner repository with the dataset identifier PXD063668 (Sample key file in Table S13). RNA-seq data are available under BioProject accession numbers PRJNA705456 (*Zea mays*) and PRJNA1260937 (*Tripsacum dactyloides*) in the NCBI BioProject database (https://www.ncbi.nlm.nih.gov/bioproject/). Genome assemblies and annotations used in this study are publicly available from MaizeGDB (Woodhouse et al., 2021) at https://maizegdb.org/PanAnd_project for *Tripsacum dactyloides* (Td-FL_9056069_6-DRAFT-PanAnd-1.0), *Andropogon gerardi* (Ag-CAM1351-DRAFT-PanAnd-1.0), and *Sorghastrum nutans* (Sn-CAM1369-DRAFT-PanAnd-1.0), and from the JGI Data Portal (Goodstein et al., 2012) at https://data.jgi.doe.gov/ for *Miscanthus* × *giganteus* (Msinensis_497_v7.0) and *Panicum virgatum* (Pvirgatumvar_WBCHAP1_778_v1.0), along with their corresponding GFF annotation files. Functional annotations, data tables, and analysis scripts are available from GitHub at https://github.com/elor77/PACMAD-Rhizome-Proteomics.

References

Abramson J, **Adler J**, **Dunger J**, **Evans R**, **Green T**, **Pritzel A**, **Ronneberger O**, **Willmore L**, **Ballard AJ**, **Bambrick J**, *et al.* **2024**. Accurate structure prediction of biomolecular interactions with AlphaFold 3. *Nature* **630**: 493–500.

Alexa A, **Rahnenfuhrer J**. **2017**. *topGO: Enrichment analysis for gene ontology*. Bioconductor.

Aroca R, **Porcel R**, **Ruiz-Lozano JM**. **2012**. Regulation of root water uptake under abiotic stress conditions. *J. Exp. Bot.* **63**: 43–57.

Arthan W, **Baker WJ**, **Barrett MD**, **Barrett RL**, **Bennetzen J**, **Besnard G**, **Bianconi M**, **Birch JL**, **Catalán P**, **Chen W**, *et al.* **2024**. Grass Phylogeny Working Group III: data repository.

Barnes AC, **Benning C**, **Roston RL**. **2016**. Chloroplast membrane remodeling during freezing stress is accompanied by cytoplasmic acidification activating SENSITIVE TO FREEZING2. *Plant Physiol.* **171**: 2140–2149.

Barnes AC, **Myers JL**, **Surber SM**, **Liang Z**, **Mower JP**, **Schnable JC**, **Roston RL**. **2023**. Oligogalactolipid production during cold challenge is conserved in early diverging lineages. *J. Exp. Bot.* **74**: 5405–5417.

Bolger AM, **Lohse M**, **Usadel B**. **2014**. Trimmomatic: a flexible trimmer for Illumina sequence data. *Bioinformatics* **30**: 2114–2120.

Brotzge JA, **Wang J**, **Thorncroft CD**, **Joseph E**, **Bain N**, **Bassill N**, **Farruggio N**, **Freedman JM**, **Hemker K**, **Johnston D**, *et al.* **2020**. A technical overview of the New York state mesonet standard network. *J. Atmos. Ocean. Technol.* **37**: 1827–1845.

Buchfink B, **Reuter K**, **Drost H-G**. **2021**. Sensitive protein alignments at tree-of-life scale using DIAMOND. *Nat Methods* **18**: 366–368.

Chen L, **Luo J**, **Jin M**, **Yang N**, **Liu X**, **Peng Y**, **Li W**, **Phillips A**, **Cameron B**, **Bernal JS**, *et al.* **2022**. Genome sequencing reveals evidence of adaptive variation in the genus Zea. *Nat. Genet.* **54**: 1736–1745.

725 **Cope AL**, **Schraiber JG**, **Pennell M**. **2025**. Macroevolutionary divergence of gene expression
726 driven by selection on protein abundance. *Science* **387**: 1063–1068.

727 **Cuevas-Velazquez CL**, **Reyes JL**, **Covarrubias AA**. **2017**. Group 4 late embryogenesis
728 abundant proteins as a model to study intrinsically disordered proteins in plants. *Plant Signal.*
729 *Behav.* **12**: e1343777.

730 **Degenkolbe T**, **Giavalisco P**, **Zuther E**, **Seiwert B**, **Hincha DK**, **Willmitzer L**. **2012**.
731 Differential remodeling of the lipidome during cold acclimation in natural accessions of
732 Arabidopsis thaliana: Lipidomics of Arabidopsis cold acclimation. *Plant J.* **72**: 972–982.

733 **Domon J-M**, **Baldwin L**, **Acket S**, **Caudeville E**, **Arnoult S**, **Zub H**, **Gillet F**, **Lejeune-**
734 **Hénaut I**, **Brancourt-Hulmel M**, **Pelloux J**, *et al.* **2013**. Cell wall compositional
735 modifications of Miscanthus ecotypes in response to cold acclimation. *Phytochemistry* **85**: 51–
736 61.

737 **Dure L 3rd**. **1993**. A repeating 11-mer amino acid motif and plant desiccation. *Plant J.* **3**: 363–
738 369.

739 **Emms DM**, **Kelly S**. **2019**. OrthoFinder: phylogenetic orthology inference for comparative
740 genomics. *Genome Biol.* **20**: 238.

741 **Fu Q**, **Liu Z**, **Bhawal R**, **Anderson ET**, **Sherwood RW**, **Yang Y**, **Thannhauser T**, **Schroyen**
742 **M**, **Tang X**, **Zhang H**, *et al.* **2021**. Comparison of MS2, synchronous precursor selection MS3,
743 and real-time search MS3 methodologies for lung proteomes of hydrogen sulfide treated swine.
744 *Anal. Bioanal. Chem.* **413**: 419–429.

745 **Gallaher TJ**, **Peterson PM**, **Soreng RJ**, **Zuloaga FO**, **Li D-Z**, **Clark LG**, **Tyrrell CD**,
746 **Welker CAD**, **Kellogg EA**, **Teisher JK**. **2022**. Grasses through space and time: An overview
747 of the biogeographical and macroevolutionary history of Poaceae. *J. Syst. Evol.* **60**: 522–569.

748 **Gault CM**, **Kremling KA**, **Buckler ES**. **2018**. Tripsacum DE novo transcriptome assemblies
749 reveal parallel gene evolution with maize after ancient polyploidy. *Plant Genome* **11**: 180012.

750 **Ginsawaeng O**, **Heise C**, **Sangwan R**, **Karcher D**, **Hernández-Sánchez IE**, **Sampathkumar**
751 **A**, **Zuther E**. **2021**. Subcellular Localization of Seed-Expressed LEA_4 Proteins Reveals
752 Liquid-Liquid Phase Separation for LEA9 and for LEA48 Homo- and LEA42-LEA48
753 Heterodimers. *Biomolecules* **11**.

754 **Goodstein DM**, **Shu S**, **Howson R**, **Neupane R**, **Hayes RD**, **Fazo J**, **Mitros T**, **Dirks W**,
755 **Hellsten U**, **Putnam N**, *et al.* **2012**. Phytozome: a comparative platform for green plant
756 genomics. *Nucleic Acids Res.* **40**: D1178-86.

757 **Hundertmark M**, **Hincha DK**. **2008**. LEA (late embryogenesis abundant) proteins and their
758 encoding genes in Arabidopsis thaliana. *BMC Genomics* **9**: 118.

759 **Iwaya-Inoue M**, **Sakurai M**, **Uemura M** (Eds). **2018**. *Survival strategies in extreme cold and*
760 *desiccation: Adaptation mechanisms and their applications*. Singapore, Singapore: Springer.

761 **Kellogg EA**. **2015**. *Flowering Plants. Monocots: Poaceae*. Cham, Switzerland: Springer
762 International Publishing.

763 **Koster KL**, **Lynch DV**. **1992**. Solute accumulation and compartmentation during the cold
764 acclimation of Puma rye. *Plant Physiol.* **98**: 108–113.

765 **Koubaa S**, **Bremer A**, **Hincha DK**, **Brini F**. **2019**. Structural properties and enzyme
766 stabilization function of the intrinsically disordered LEA_4 protein TdLEA3 from wheat. *Sci.*
767 *Rep.* **9**: 3720.

768 **Kovacs D**, **Agoston B**, **Tompa P**. **2008**. Disordered plant LEA proteins as molecular
769 chaperones. *Plant Signal. Behav.* **3**: 710–713.

770 **Li Q**, **Xiang C**, **Xu L**, **Cui J**, **Fu S**, **Chen B**, **Yang S**, **Wang P**, **Xie Y**, **Wei M**, *et al.* **2020**.
771 SMRT sequencing of a full-length transcriptome reveals transcript variants involved in C18
772 unsaturated fatty acid biosynthesis and metabolism pathways at chilling temperature in
773 Pennisetum giganteum. *BMC Genomics* **21**: 52.

774 **Liu Y**, **Liang J**, **Sun L**, **Yang X**, **Li D**. **2016**. Group 3 LEA Protein, ZmLEA3, Is Involved in
775 Protection from Low Temperature Stress. *Front. Plant Sci.* **7**: 1011.

776 **Liu Y**, **Wang L**, **Xing X**, **Sun L**, **Pan J**, **Kong X**, **Zhang M**, **Li D**. **2013**. ZmLEA3, a
777 multifunctional group 3 LEA protein from maize (Zea mays L.), is involved in biotic and
778 abiotic stresses. *Plant Cell Physiol.* **54**: 944–959.

779 **Love MI**, **Huber W**, **Anders S**. **2014**. Moderated estimation of fold change and dispersion for
780 RNA-seq data with DESeq2. *Genome Biol.* **15**: 550.

781 **Lyons JM**. **1973**. Chilling injury in plants. *Annu. Rev. Plant Physiol.* **24**: 445–466.

782 **Marks RA**, **Van Der Pas L**, **Schuster J**, **Gilman IS**, **VanBuren R**. **2024**. Convergent
783 evolution of desiccation tolerance in grasses. *Nat Plants* **10**: 1112–1125.

784 **Marrs KA**. **1996**. The functions and regulation of glutathione s-transferases in plants. *Annu*
785 *Rev Plant Physiol Plant Mol Biol* **47**: 127–158.

786 **Mori K**, **Renhu N**, **Naito M**, **Nakamura A**, **Shiba H**, **Yamamoto T**, **Suzaki T**, **Iida H**, **Miura**
787 **K**. **2018**. Ca2+-permeable mechanosensitive channels MCA1 and MCA2 mediate cold-
788 induced cytosolic Ca2+ increase and cold tolerance in Arabidopsis. *Sci. Rep.* **8**: 550.

789 **Nakashima K**, **Yamaguchi-Shinozaki K**. **2006**. Regulons involved in osmotic stress-
790 responsive and cold stress-responsive gene expression in plants. *Physiol. Plant.* **126**: 62–71.

791 **NDong C**, **Danyluk J**, **Wilson KE**, **Pocock T**, **Huner NPA**, **Sarhan F**. **2002**. Cold-regulated
792 cereal chloroplast late embryogenesis abundant-like proteins. Molecular characterization and
793 functional analyses. *Plant Physiol* **129**: 1368–1381.

794 **Ojeda-Rivera JO**, **Barnes AC**, **Ainsworth EA**, **Angelovici R**, **Basso B**, **Brindisi LJ**, **Brooks**
795 **MD**, **Busch W**, **Buttelmann GL**, **Castellano MJ**, *et al.* **2025**. Designing a nitrogen-efficient
796 cold-tolerant maize for modern agricultural systems. *Plant Cell* **37**.

797 **Orvar BL**, **Sangwan V**, **Omann F**, **Dhindsa RS**. **2000**. Early steps in cold sensing by plant
798 cells: the role of actin cytoskeleton and membrane fluidity. *Plant J.* **23**: 785–794.

799 **Pearce R**. **2001**. Plant Freezing and Damage. *Ann. Bot.* **87**: 417–424.

800 **Perez-Riverol Y**, **Bandla C**, **Kundu DJ**, **Kamatchinathan S**, **Bai J**, **Hewapathirana S**, **John**
801 **NS**, **Prakash A**, **Walzer M**, **Wang S**, *et al.* **2025**. The PRIDE database at 20 years: 2025
802 update. *Nucleic Acids Res.* **53**: D543–D553.

803 **Popova AV**, **Rausch S**, **Hundertmark M**, **Gibon Y**, **Hincha DK**. **2015**. The intrinsically
804 disordered protein LEA7 from Arabidopsis thaliana protects the isolated enzyme lactate
805 dehydrogenase and enzymes in a soluble leaf proteome during freezing and drying. *Biochim.*
806 *Biophys. Acta* **1854**: 1517–1525.

807 **Puhakainen T**, **Hess MW**, **Mäkelä P**, **Svensson J**, **Heino P**, **Palva ET**. **2004**. Overexpression
808 of multiple dehydrin genes enhances tolerance to freezing stress in Arabidopsis. *Plant Mol.*
809 *Biol.* **54**: 743–753.

810 **Ranaweera T**, **Brown BNI**, **Wang P**, **Shiu S-H**. **2022**. Temporal regulation of cold
811 transcriptional response in switchgrass. *Front. Plant Sci.* **13**: 998400.

812 **Roeder AHK**, **Shi Y**, **Yang S**, **Abbas M**, **Sasidharan R**, **Yanovsky MJ**, **Casal JJ**, **Ruffel S**,
813 **von Wirén N**, **Assmann SM**, *et al.* **2025**. Translational insights into abiotic interactions: From
814 Arabidopsis to crop plants. *Plant Cell* **37**: koaf140.

815 **Romero-Pérez PS**, **Martínez-Castro LV**, **Linares A**, **Arroyo-Mosso I**, **Sánchez-Puig N**,
816 **Cuevas-Velazquez CL**, **Sukenik S**, **Guerrero A**, **Covarrubias AA**. **2024**. Self-association
817 and multimer formation in AtLEA4-5, a desiccation-induced intrinsically disordered protein
818 from plants. *Protein Sci* **33**: e5192.

819 **Sage RF**, **Christin P-A**, **Edwards EJ**. **2011**. The C(4) plant lineages of planet Earth. *J. Exp.*
820 *Bot.* **62**: 3155–3169.

821 **Sapay N**, **Guermeur Y**, **Deléage G**. **2006**. Prediction of amphipathic in-plane membrane
822 anchors in monotopic proteins using a SVM classifier. *BMC Bioinformatics* **7**: 255.

823 **Schat L**, **Schubert M**, **Fjellheim S**, **Humphreys AM**. **2025**. Drought tolerance as an
824 evolutionary precursor to frost and winter tolerance in grasses. *Evolution* **79**: 541–556.

825 **Schubert M**, **Grønvold L**, **Sandve SR**, **Hvidsten TR**, **Fjellheim S**. **2019**. Evolution of cold
826 acclimation and its role in niche transition in the temperate grass subfamily Pooideae. *Plant*
827 *Physiol.* **180**: 404–419.

828 **Schubert M**, **Humphreys AM**, **Lindberg CL**, **Preston JC**, **Fjellheim S**. **2020**. To*coldly*go
829 where no grass has gone before: A multidisciplinary review of cold adaptation in Poaceae.
830 *Annual Plant Reviews online*: 523–562.

831 **Singh KK**, **Graether SP**. **2021**. The in vitro structure and functions of the disordered late
832 embryogenesis abundant three proteins. *Protein Sci.* **30**: 678–692.

833 **Stitzer MC**, **Seetharam AS**, **Scheben A**, **Hsu S-K**, **Schulz AJ**, **AuBuchon-Elder TM**, **El-**
834 **Walid M**, **Ferebee TH**, **Hale CO**, **La T**, *et al.* **2025**. Extensive genome evolution distinguishes
835 maize within a stable tribe of grasses. *bioRxivorg*: 2025.01. 22.633974.

836 **Stolsmo SP**, **Lindberg CL**, **Ween RE**, **Schat L**, **Preston JC**, **Humphreys AM**, **Fjellheim S**.
837 **2024**. Evolution of drought and frost responses in cool season grasses (Pooideae): was drought
838 tolerance a precursor to frost tolerance? *J. Exp. Bot.* **75**: 6405–6422.

839 **Sun W**, **Van Montagu M**, **Verbruggen N**. **2002**. Small heat shock proteins and stress
840 tolerance in plants. *Biochim Biophys Acta* **1577**: 1–9.

841 **Suzuki N**, **Mittler R**. **2006**. Reactive oxygen species and temperature stresses: A delicate
842 balance between signaling and destruction. *Physiol. Plant.* **126**: 45–51.

843 **Takamori LM**, **Pereira AVC**, **Maia Souza G**, **Vieira LGE**, **Ferreira Ribas A**. **2017**.
844 Identification of endogenous reference genes for RT-qPCR expression analysis in Urochloa
845 brizantha under abiotic stresses. *Sci. Rep.* **7**: 8502.

846 **Thomashow MF**. **1999**. PLANT COLD ACCLIMATION: Freezing tolerance genes and
847 regulatory mechanisms. *Annu. Rev. Plant Physiol. Plant Mol. Biol.* **50**: 571–599.

848 **Törönen P**, **Holm L**. **2022**. PANNZER-A practical tool for protein function prediction.
849 *Protein Sci* **31**: 118–128.

850 **Vera-Hernández P**, **Ortega Ramírez MA**, **Martínez Núñez M**, **Ruiz-Rivas M**, **Rosas-**
851 **Cárdenas F de F**. **2018**. Proline as a probable biomarker of cold stress tolerance in Sorghum
852 (Sorghum bicolor). *Mex. J. Biotechnol.* **3**: 77–86.

853 **Woodhouse MR**, **Cannon EK**, **Portwood JL 2nd**, **Harper LC**, **Gardiner JM**, **Schaeffer**
854 **ML**, **Andorf CM**. **2021**. A pan-genomic approach to genome databases using maize as a model
855 system. *BMC Plant Biol.* **21**: 385.

856 **Wu B**, **Luo D**, **Yue Y**, **Yan H**, **He M**, **Ma X**, **Zhao B**, **Xu B**, **Zhu J**, **Wang J**, *et al.* **2024**.
857 Haplotype-resolved genome assembly of upland switchgrass provides insights into cold
858 tolerance. *bioRxiv*: 2024.08.26.609807.

859 **Xie Z**, **Lin W**, **Yu G**, **Cheng Q**, **Xu B**, **Huang B**. **2019**. Improved cold tolerance in switchgrass
860 by a novel CCCH-type zinc finger transcription factor gene, PvC3H72, associated with ICE1-
861 CBF-COR regulon and ABA-responsive genes. *Biotechnol. Biofuels* **12**: 224.

862 **Xu K**, **Zhao Y**, **Gu J**, **Zhou M**, **Gao L**, **Sun R-X**, **Wang W-W**, **Zhang S-H**, **Yang X-J**. **2022**.
863 Proteomic analysis reveals the molecular mechanism underlying the cold acclimation and
864 freezing tolerance of wheat (*Triticum aestivum* L.). *Plant Sci.* **318**: 111242.

865 **Xue C**, **Jiang Y**, **Wang Z**, **Shan X**, **Yuan Y**, **Hua J**. **2021**. Tissue-level transcriptomic
866 responses to local and distal chilling reveal potential chilling survival mechanisms in maize. *J.*
867 *Exp. Bot.* **72**: 7610–7625.

868 **Zhang Y**, **Ngu DW**, **Carvalho D**, **Liang Z**, **Qiu Y**, **Roston RL**, **Schnable JC**. **2017**.
869 Differentially regulated orthologs in sorghum and the subgenomes of maize. *Plant Cell* **29**:
870 1938–1951.

871

872 **Supporting Information**

873 The following Supporting Information is available for this article:

874 **Fig. S1** Rhizome morphology at sampling.

875 **Fig. S2** Principal component analysis of log-transformed protein abundance data.

876 **Fig. S3** Biological processes (BPs) within curated cold-related functional categories.

877 **Fig. S4** Volcano plots showing differentially accumulated proteins in sampled species.

878 **Fig. S5** Upset plots of shared differentially accumulated proteins among species in winter and
879 summer.

880 **Fig. S6** Enriched BPs in rhizomes of five PACMAD grass species and BP distribution within
881 curated cold-related functional categories.

882 **Fig. S7** Scatterplots showing the relationship between rhizome proteins and cold-responsive
883 mRNA expression in *Tripsacum* and maize tissues.

884 **Fig. S8** MAFFT alignment of LEA3 across six PACMAD species.

885 **Fig. S9** Hydropathy profiles of LEA3 orthologs.

886 **Fig. S10** AlphaFold 3 prediction of LEA3 homo-tetramer assemblies in *Tripsacum* and *Zea*
887 *mays.*

888 **Table S1** Normalized protein abundances (log_2-transformed) for all samples.

889 **Table S2** Genome assembly statistics for the five species analyzed.

890 **Table S3** List of 4,888 orthogroups identified across species.

891 **Table S4** Log_2 fold-changes (Winter/Summer) for all quantified proteins.

892 **Table S5** GO enrichment analysis for winter-upregulated proteins.

893 **Table S6** GO enrichment analysis for winter-downregulated proteins.

894 **Table S7** Top 50 most abundant proteins in winter vs summer.

895 **Table S8** Elongation Factor 1-alpha (EF1) orthologs and abundance data.

896 **Table S9** Heat Shock Protein (HSP) orthologs and abundance data.

897 **Table S10** LEA3 orthologs and abundance data.

898 **Table S11** Hydrophobicity scores for LEA3 orthologs.

899 **Table S12** Biophysical properties of individual 11mer LEA3 (OG0022470) tandem repeats.

900 **Table S13** PRIDE sample key and metadata.

901 **Methods S1** Detailed protocols for protein extraction, S-Trap digestion, LC–MS/MS search
902 parameters, RNA-seq alignment settings, and bioinformatics pipeline parameters.

903 **Code S1** R script for importing original Ag/Mg multiplexed peptide intensities.

904 **Code S2** R script for re-aligning peptides using DIAMOND.

905 **Code S3** R script for summarizing peptides into protein-level data.